DOI: 10.3901/CJME.2011.06.***, available online at www.cjmenet.com; www.cjmenet.com.cn

Study on Nonlinear Dynamic Characteristics of the Vectored Thruster AUV in Complex Sea Conditions

GAO Fudong*, PAN Cunyun, XU Xiaojun, ZHANG Xiang

College of Mechatronic Engineering and Automation,
National University of Defense Technology, Changsha 410073, China

Received November 17, 2010; revised June 22, 2011; accepted July 1, 2011; published electronically July 12, 2011

Abstract: The mobility of the vectored thruster AUV in different environment is the important premise of control system design. The new type of autonomous underwater vehicle (AUV) equipped with rudders and vectored thrusters which are combined to control the course is studied. Firstly, Euler angles representation and quaternion method are applied to establish six-DOF kinematic model respectively, then Newton second law and Lagrangian approach are used to deduce the vectored thruster AUV's nonlinear dynamic equations with six degrees of freedom (DOF) respectively in complex sea conditions based on the random wave theory according to the structural and kinetic characteristics of the vectored thruster AUV in this paper. The kinematic models and dynamic models based on different theories have the same expression and conclusion, which shows that the kinematic models and dynamic models of the vectored thruster AUV are accurate. The Runge-Kutta arithmetic is used to solve the dynamic equations, which not only can simulate the motions such as cruise and hover but also can describe the vehicle's low-frequency and high-frequency motion. The results of computation show that the mobility of the vectored thruster AUV in interference-free environment and the integrated signals including low-frequency motion signal and high-frequency motion signal in environmental disturbance accord with practical situation, which not only solve the problem of especial singularities when the pitch angle $\theta = \pm 90°$ but also clears up the difficulties of computation and display of the coupled nonlinear motion equations in complex sea conditions. Moreover, the high maneuverability of the vectored thruster AUV equipped with rudders and vectored thrusters is validated, which lays a foundation for the control system design.

Key words: complex sea conditions, vectored thruster, autonomous underwater vehicle, nonlinear dynamic characteristics

1 Introduction

AUVs are promising vehicles for navy because they can fulfill many missions such as underwater work and accurate underwater attack. Therefore, it is required to have high mobility and maneuverability. Nowadays, how to enhance the maneuverability of AUVs is an important issue in the domain of international navigation in that most AUVs just have a single function of underwater navigation or submarine movement. The university of Tianjin has designed an AUV with capabilities of landing and sitting-bottom, which got ahead[1]. The vectored thruster AUV in this paper makes use of the flexible transmission shaft based on spherical gear as the kinetic source equipment, on the end of that a new wheel propeller is installed[2, 3]. The whole equipment can achieve four functions such as wheels, legs, thrusters and course control based on the characteristics of spatial deflexion and continual circumgyratetion of the flexible transmission shaft, which makes the vectored thruster AUV fulfill multi-moving states in amphibian conditions, shown in Fig. 1. In order to improve the efficiency of course control, four vector thrusters are used to control the course in the low-speed navigation and rudders are used to control the course in high-speed navigation. So the vectored thruster AUV has more flexible mobility with its complex form of movements compared with the control-configured underwater vehicles. The AUV's mathematical model of space motion is the basic premise and important basis for some research such as overall performance, control systems, guidance law and so on. In order to facilitate calculation and analysis, domestic and foreign scholars usually separated the six-DOF space motion of underwater vehicles into vertical and horizontal plane motions to research respectively, this simplification is still able to meet the underwater vehicles of less demanding mobility and little cross-linked effect on motion[4–6]. With the development of underwater vehicles, the simplified motion models used in the past can not meet the higher demands of mobility, control quality and guidance precision, so a complete spatial motion model of underwater vehicles needs to be established. At present, the six-DOF motion equations of underwater vehicles are extremely complex and strongly

* Corresponding author. E-mail: gaofudong2005@163.com
This project is supported by National Hi-tech Research and Development Program of China(863 Program, Grant No. 2006AA09Z235), and Hunan Provincial Innovation Foundation For Postgraduate of China(Grant No. CX2009B003)

coupled[7–8], when they are calculated in the simulink toolbox of Matlab software, not only the computational speed is decreased due to the coupling of the motion parameters, but also the calculation will be failed duo to the algebraic loop problems. The motion of underwater vehicles in complex sea conditions is complicated, which is separated into two parts including low frequency motion and high frequency motion. The low-frequency motion is caused by ocean current, second-order wave force and propulsion, while high-frequency motion is caused by the first-order wave force[9]. The high-frequency motion will not change the average position of underwater vehicles because it only represented periodical oscillating movement. In order to avoid that the energy is waste and the propellers are wore down, the high-frequency motion signal should be filtered from the integrated motion signal so that the low-frequency motion signal is controlled and the high-frequency motion signal is uncontrolled.

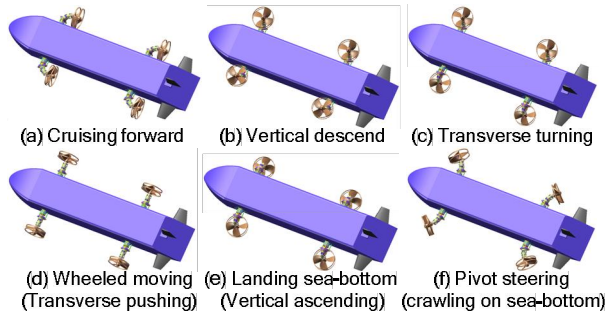

Fig. 1. Typical motions of the vectored thruster AUV

In this paper, according to the structural and kinetic characteristics of the vectored thruster AUV, the vector modeling method based on random wave theory is applied to establish six-DOF nonlinear kinematic and dynamic models in complex sea conditions through unifying the movement parameters to reduce the coupling between them. Then the Runge-Kutta arithmetic is used to solve the nonlinear kinematic and dynamic equations so that the mobility of the vectored thruster AUV in interference-free environment is analyzed and its integrated signals including low-frequency motion signal and high-frequency motion signal in environmental disturbance are obtained.

2 Six-DOF Nonlinear Kinematic Model

2.1 Euler angles for kinematics modeling

In order to describe the movement of the vectored thruster AUV, the inertial coordinate system E-$\xi\eta\zeta$ and body-fixed coordinate system B-xyz are used, shown in Fig. 2. The origin B of body-fixed coordinate system is 0.003 m after the center of buoyancy. The vectored thruster AUV has two planes of symmetry and the body's symmetry axes coincide with the principal axes of inertia, so the inertia tensor of the body-fixed coordinate system is diagonal. The kinematic parameters include $\boldsymbol{\eta}$ that denotes the position and attitude vector with coordinates in the inertial coordinate system, $\boldsymbol{v}$ that denotes the linear and angular velocity vector with coordinates in the body-fixed coordinate system and $\boldsymbol{f}$ that describes the forces and moments acting on the vehicle in the body-fixed coordinate system, the specific forms can be written as follows:

$$\boldsymbol{\eta}=\left(\boldsymbol{\eta}_1^{\mathrm{T}},\boldsymbol{\eta}_2^{\mathrm{T}}\right)^{\mathrm{T}},\ \boldsymbol{\eta}_1=\left(\xi,\eta,\zeta\right)^{\mathrm{T}},\ \boldsymbol{\eta}_2=\left(\phi,\theta,\psi\right)^{\mathrm{T}};$$
$$\boldsymbol{v}=\left(\boldsymbol{v}_1^{\mathrm{T}},\boldsymbol{v}_2^{\mathrm{T}}\right)^{\mathrm{T}},\ \boldsymbol{v}_1=\left(u,v,w\right)^{\mathrm{T}},\ \boldsymbol{v}_2=\left(p,q,r\right)^{\mathrm{T}};$$
$$\boldsymbol{f}=\left(\boldsymbol{f}_1^{\mathrm{T}},\boldsymbol{f}_2^{\mathrm{T}}\right)^{\mathrm{T}},\ \boldsymbol{f}_1=\left(X,Y,Z\right)^{\mathrm{T}},\ \boldsymbol{f}_2=\left(K,M,N\right)^{\mathrm{T}}.$$

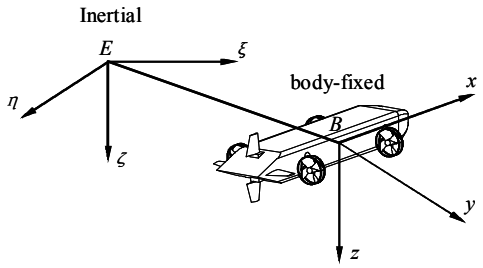

Fig. 2. Inertial and body-fixed coordinate systems

The inertial coordinate system can coincide with the body-fixed coordinate system through three times rotations about ξ axis, η axis and ζ axis respectively according to the definition of Euler angles, shown in Fig. 3. Firstly, let $\xi'\eta'\zeta$ be the coordinate system obtained by translating the inertial coordinate system $\xi\eta\zeta$ parallel to itself until its origin coincides with the origin of the body-fixed coordinate system. Then the coordinate system $\xi'\eta'\zeta$ is rotated a pitch angle θ about the η' axis, this yields the coordinate system $x\eta'\zeta'$. Finally, the coordinate system $x\eta'\zeta'$ is rotated a roll angle ϕ about the x axis, this yields the coordinate system xyz. So the transformation matrix that transforms the coordinates (x, y, z) of body-fixed coordinate system into that of inertial coordinate system is written as follows:

$$\boldsymbol{J}_1\left(\boldsymbol{\eta}_2\right)=\begin{pmatrix}\mathrm{c}\psi\,\mathrm{c}\theta & \mathrm{c}\psi\,\mathrm{s}\theta\,\mathrm{s}\phi-\mathrm{s}\psi\,\mathrm{c}\phi & \mathrm{c}\psi\,\mathrm{s}\theta\,\mathrm{c}\phi+\mathrm{s}\psi\,\mathrm{s}\phi\\ \mathrm{s}\psi\,\mathrm{c}\theta & \mathrm{s}\psi\,\mathrm{s}\theta\,\mathrm{s}\phi+\mathrm{c}\psi\,\mathrm{c}\phi & \mathrm{s}\psi\,\mathrm{s}\theta\,\mathrm{c}\phi-\mathrm{c}\psi\,\mathrm{s}\phi\\ -\mathrm{s}\theta & \mathrm{c}\theta\,\mathrm{s}\phi & \mathrm{c}\theta\,\mathrm{c}\phi\end{pmatrix},\quad(1)$$

where s·=sin(·) and c·=cos(·).

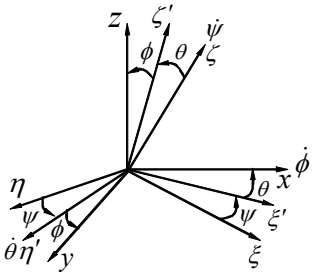

Fig. 3. Rotational sequence of the coordinate systems

These parameters as $\boldsymbol{x}$, $\boldsymbol{y}$, $\boldsymbol{z}$, $\boldsymbol{\eta}'$, $\boldsymbol{\eta}$, $\boldsymbol{\xi}$, and $\boldsymbol{\zeta}$ are all unit vectors. So the angular velocity in the inertial coordinate system is expressed as

$$\boldsymbol{\Omega} = \dot{\phi}\boldsymbol{x} + \dot{\theta}\boldsymbol{\eta}' + \dot{\psi}\boldsymbol{\zeta} . \tag{2}$$

The inertial coordinate system rotates for the first time can be written as

$$\dot{\theta}\boldsymbol{\eta}' = -\dot{\theta}\sin\psi\boldsymbol{\xi} + \dot{\theta}\cos\psi\boldsymbol{\eta} . \tag{3}$$

Further, the following transformation relations can be obtained:

$$\begin{cases} \dot{\phi} = p + q\sin\phi\tan\theta + r\cos\phi\tan\theta \\ \dot{\theta} = q\cos\phi - r\sin\phi \\ \dot{\psi} = q\sin\phi\sec\theta + r\cos\phi\sec\theta \end{cases} . \tag{4}$$

Therefore, the transformation matrix that transforms the coordinates (p, q, r) of body-fixed coordinate system into that of inertial coordinate system is written as

$$\boldsymbol{J}_2(\boldsymbol{\eta}_2) = \begin{pmatrix} 1 & \sin\phi\tan\theta & \cos\phi\tan\theta \\ 0 & \cos\phi & -\sin\phi \\ 0 & \sin\phi\sec\theta & \cos\phi\sec\theta \end{pmatrix} . \tag{5}$$

In summary, the six-DOF kinematics equation of the vectored thruster AUV can be written as

$$\begin{pmatrix} \dot{\boldsymbol{\eta}}_1 \\ \dot{\boldsymbol{\eta}}_2 \end{pmatrix} = \begin{pmatrix} \boldsymbol{J}_1(\boldsymbol{\eta}_2) & 0_{3\times3} \\ 0_{3\times3} & \boldsymbol{J}_2(\boldsymbol{\eta}_2) \end{pmatrix} \begin{pmatrix} \boldsymbol{v}_1 \\ \boldsymbol{v}_2 \end{pmatrix} . \tag{6}$$

2.2 Quaternion method for kinematics modeling

The Euler angles for kinematics modeling will bring singular points in special circumstances when the pitch angles get ±90° in Eq. (5). In order to solve this problem, the quaternion method can be used for kinematics modeling.

In order to avoid the appearance of singular points, the quaternion method use the plural form express the Euler angles. Similarly, the coordinate transformation has the following form:

$$\begin{pmatrix} \dot{\boldsymbol{\eta}}_1 \\ \dot{e} \end{pmatrix} = \begin{pmatrix} \boldsymbol{E}_1(e) & 0_{3\times3} \\ 0_{4\times3} & \boldsymbol{E}_2(e) \end{pmatrix} \begin{pmatrix} \boldsymbol{v}_1 \\ \boldsymbol{v}_2 \end{pmatrix} , \tag{7}$$

where a quaternion can be expressed as a vector $\boldsymbol{e} = (\varepsilon_1, \varepsilon_2, \varepsilon_3, \varepsilon_4)^{\mathrm{T}}$ and it satisfies that

$$\varepsilon_1^2 + \varepsilon_2^2 + \varepsilon_3^2 + \varepsilon_4^2 = 1 . \tag{8}$$

The transformation matrix $\boldsymbol{E}_1(\boldsymbol{e})$ and $\boldsymbol{E}_2(\boldsymbol{e})$ are composed of the parameters ε_1, ε_2, ε_3 and ε_4, the specific forms are

$$\boldsymbol{E}_1(\boldsymbol{e}) = \begin{pmatrix} 1-2\left(\varepsilon_2^2+\varepsilon_3^2\right) & 2\left(\varepsilon_1\varepsilon_2-\varepsilon_3\varepsilon_4\right) & 2\left(\varepsilon_1\varepsilon_3+\varepsilon_2\varepsilon_4\right) \\ 2\left(\varepsilon_1\varepsilon_2+\varepsilon_3\varepsilon_4\right) & 1-2\left(\varepsilon_1^2+\varepsilon_3^2\right) & 2\left(\varepsilon_2\varepsilon_3-\varepsilon_1\varepsilon_4\right) \\ 2\left(\varepsilon_1\varepsilon_3-\varepsilon_2\varepsilon_4\right) & 2\left(\varepsilon_2\varepsilon_3+\varepsilon_1\varepsilon_4\right) & 1-2\left(\varepsilon_1^2+\varepsilon_2^2\right) \end{pmatrix} , \tag{9}$$

$$\boldsymbol{E}_2(\boldsymbol{e}) = \frac{1}{2}\begin{pmatrix} \varepsilon_4 & -\varepsilon_3 & \varepsilon_2 \\ \varepsilon_3 & \varepsilon_4 & -\varepsilon_1 \\ -\varepsilon_2 & \varepsilon_1 & \varepsilon_4 \\ -\varepsilon_1 & -\varepsilon_2 & -\varepsilon_3 \end{pmatrix} . \tag{10}$$

The computation of initial value $\boldsymbol{\eta}_1(0)$ and $\boldsymbol{e}(0)$ is the key issue in quaternion method, Shepherd proposed that the quaternion can be computed by means of Euler angles in 1978[10]. Assume that the initial Euler angles ϕ_0, θ_0 and ψ_0 are given, the transformation matrix $\boldsymbol{J}_1(\boldsymbol{\eta}_2)$ can be obtained, then the trace of $\boldsymbol{J}_1(\boldsymbol{\eta}_2)$ is computed according to $J_{44} = \mathrm{trace}(\boldsymbol{J}_1) = \sum_{j=1}^{3} J_{jj}$ and let $1 \le i \le 4$ be the index corresponding to $J_{ii} = \max\left(J_{11}, J_{22}, J_{33}, J_{44}\right)$. Define $\boldsymbol{p} = \left(p_1, p_2, p_3, p_4\right)^{\mathrm{T}}$ and $|p_i| = \sqrt{1 + 2J_{ii} - J_{44}}$, where the sign ascribed to p_i can be chosen either plus or minus, then compute the other three p-values from

$$\begin{aligned} &p_4p_1 = J_{32} - J_{23},\ p_4p_2 = J_{13} - J_{31},\ p_4p_3 = J_{21} - J_{12}, \\ &p_2p_3 = J_{32} + J_{23},\ p_3p_1 = J_{13} + J_{31},\ p_1p_2 = J_{21} + J_{12} . \end{aligned} \tag{11}$$

Finally, compute the initial quaternion by the following formula, the final quaternion can be computed applying the linear discrete-time algorithm:

$$\boldsymbol{e} = \frac{\boldsymbol{p}}{2} = \left(\frac{p_1}{2}, \frac{p_2}{2}, \frac{p_3}{2}, \frac{p_4}{2}\right)^{\mathrm{T}} . \tag{12}$$

Moreover, the relationship between the Euler angles and the quaternion can be established by requiring that the Rotational matrices of the two kinematic representations are equal:

$$\boldsymbol{J}_1(\boldsymbol{\eta}_2) = \boldsymbol{E}_1(\boldsymbol{e}) . \tag{13}$$

3 Nonlinear Dynamic Model of the Vectored Thruster AUV in Complex Sea Conditions

3.1 Forces and moments on the vectored thruster AUV

There are many parameters need to be identified of the vectored thruster AUV in the complex sea conditions, because it is a complicated nonlinear dynamic system. The vectored thruster AUV in this paper adopts NPS Ⅱ AUV's figure, whose accurate hydrodynamic coefficients have been obtained from the experiment[11]. The influence of the gravity, buoyancy, vectored thrust, rudder control forces, ocean current forces and wave disturbances are considered so as to establish a more integrated six-DOF dynamics model.

The gravitational force and buoyant force on the vectored thruster AUV are called restoring forces, so the restoring forces and moments vector in the body-fixed coordinate system can be expressed as follows:

$$\boldsymbol{G}(\boldsymbol{\eta})=\begin{pmatrix}\boldsymbol{f}_{\mathrm{G}}(\boldsymbol{\eta})+\boldsymbol{f}_{\mathrm{B}}(\boldsymbol{\eta})\\ \boldsymbol{R}_{\mathrm{G}}\times\boldsymbol{f}_{\mathrm{G}}(\boldsymbol{\eta})+\boldsymbol{R}_{\mathrm{B}}\times\boldsymbol{f}_{\mathrm{B}}(\boldsymbol{\eta})\end{pmatrix}=\begin{pmatrix}(B-G)\mathrm{s}\theta\\ (G-B)\mathrm{c}\theta\mathrm{s}\phi\\ (G-B)\mathrm{c}\theta\mathrm{c}\phi\\ (y_{\mathrm{G}}G-y_{\mathrm{B}}B)\mathrm{c}\theta\mathrm{c}\phi-(z_{\mathrm{G}}G-z_{\mathrm{B}}B)\mathrm{c}\theta\mathrm{s}\phi\\ -(z_{\mathrm{G}}G-z_{\mathrm{B}}B)\mathrm{s}\theta-(x_{\mathrm{G}}G-x_{\mathrm{B}}B)\mathrm{c}\theta\mathrm{c}\phi\\ (x_{\mathrm{G}}G-x_{\mathrm{B}}B)\mathrm{c}\theta\mathrm{s}\phi+(y_{\mathrm{G}}G-y_{\mathrm{B}}B)\mathrm{s}\theta\end{pmatrix}, \quad (14)$$

where s·=sin(·) and c·=cos(·), $\boldsymbol{f}_{\mathrm{G}}(\boldsymbol{\eta})$ is the gravity vector in the body-fixed coordinate system, $\boldsymbol{f}_{\mathrm{B}}(\boldsymbol{\eta})$ is the buoyancy vector in the body-fixed coordinate system, $\boldsymbol{R}_{\mathrm{G}}$ is the position vector of the center of gravity in the body-fixed coordinate system, $\boldsymbol{R}_{\mathrm{B}}$ is the position vector of the center of buoyancy in the body-fixed coordinate system, G is the gravity scalar in the inertial coordinate system, B is the buoyancy scalar in the inertial coordinate system. In order to facilitate the deduction of formulae, define that $\boldsymbol{g}(\boldsymbol{\eta}) = -\boldsymbol{G}(\boldsymbol{\eta})$.

The CFD method is used to simulate numerically the open-water performance of the wheel propeller[12], then the least squares curve fitting approach is used to deal with the computational data. So the expressions of thrust coefficient K_{t} and torque coefficient K_{q} about the advance coefficient J of the wheel propeller are obtained:

$$\begin{cases}K_{\mathrm{t}}=K_0+K_1J+K_2J^2\\ K_{\mathrm{q}}=\overline{K}_0+\overline{K}_1J+\overline{K}_2J^2\end{cases}, \quad (15)$$

where the parameters K_0, K_1, K_2, $\overline{K}_0$, $\overline{K}_1$ and $\overline{K}_2$ are all constants.

In order to make the operating characteristics of the wheel propeller closer to the real situation, the wake coefficient and the thrust deduction factor are considered because of the interaction between the wheel propellers and the vectored thruster AUV, so the thrust T_{e} and torque Q_{p} can be expressed as follows:

$$\begin{cases}T_{\mathrm{e}}=A_0U^2+B_0Un+C_0n^2\\ Q_{\mathrm{p}}=\overline{A}_0U^2+\overline{B}_0Un+\overline{C}_0n^2\end{cases}, \quad (16)$$

where $A_0=(1-t)(1-w_{\mathrm{p}})^2\rho D^2K_2$, $B_0=(1-t)(1-w_{\mathrm{p}})\rho D^3K_1$, $C_0=(1-t)\rho D^4K_0$, $\overline{A}_0=(1-w_{\mathrm{p}})^2\rho D^3\overline{K}_2$, $\overline{C}_0=\rho D^5\overline{K}_0$, $\overline{B}_0=(1-w_{\mathrm{p}})\rho D^4\overline{K}_1$, n is the propeller rotational speed, U is the speed of the vectored thruster AUV, t is the thrust deduction factor, w_{p} is the wake coefficient, D is the propeller diameter.

The thrust $\boldsymbol{T}$ of a three-DOF vectored thruster is a vector which can adjust the direction according to the course control need of the vectored thruster AUV, as shown in Fig. 4. The expressions of a single vectored thrust $\boldsymbol{T}$ through decomposing it can be written:

$$\begin{cases}T_{x_i}=T_{\mathrm{e}}\cos\delta_{\mathrm{d}_i}\cos\delta_{\mathrm{f}_i}\\ T_{y_i}=T_{\mathrm{e}}\cos\delta_{\mathrm{d}_i}\sin\delta_{\mathrm{f}_i}\\ T_{z_i}=T_{\mathrm{e}}\sin\delta_{\mathrm{d}_i}\end{cases}. \quad (17)$$

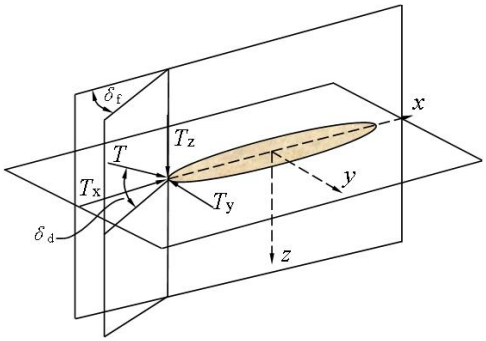

Fig. 4. Thrust orientation of a vectored thruster

The total thrust and total torque of four vectored thrusters can be written as follows:

$$\boldsymbol{f}_{\mathrm{p}}=\begin{pmatrix}T_x\\ T_y\\ T_z\\ Q_x\\ Q_y\\ Q_z\end{pmatrix}=\begin{pmatrix}T_{x_1}+T_{x_2}+T_{x_3}+T_{x_4}\\ T_{y_1}+T_{y_2}+T_{y_3}+T_{y_4}\\ T_{z_1}+T_{z_2}+T_{z_3}+T_{z_4}\\ Q_{x_1}+Q_{x_2}+Q_{x_3}+Q_{x_4}\\ Q_{y_1}+Q_{y_2}+Q_{y_3}+Q_{y_4}\\ Q_{z_1}+Q_{z_2}+Q_{z_3}+Q_{z_4}\end{pmatrix}. \quad (18)$$

The rudders of the vectored thruster AUV are used to control the course in high-speed navigation, whose forces and moments are

$$\boldsymbol{f}_{\mathrm{r}}=\begin{pmatrix} M & N \\ 0 & Y_{u|u|\delta_{\mathrm{r}}}u|u| \\ Z_{u|u|\delta_{\mathrm{p}}}u|u| & 0 \\ 0 & K_{u|u|\delta_{\mathrm{r}}}u|u| \\ M_{u|u|\delta_{\mathrm{p}}}u|u| & 0 \\ 0 & N_{u|u|\delta_{\mathrm{r}}}u|u| \end{pmatrix}\begin{pmatrix}\delta_{\mathrm{p}}\\ \delta_{\mathrm{r}}\end{pmatrix}. \tag{19}$$

where δ_{p} is the plane angle and δ_{r} is the rudder angle,

$M=X_{uq\delta_{\mathrm{p}}}uq+X_{uw\delta_{\mathrm{p}}}uw+u|u|X_{u|u|\delta_{\mathrm{p}}\delta_{\mathrm{p}}}\delta_{\mathrm{p}}$,

$N=X_{ur\delta_{\mathrm{r}}}ur+X_{uv\delta_{\mathrm{r}}}uv+u|u|X_{u|u|\delta_{\mathrm{r}}\delta_{\mathrm{r}}}\delta_{\mathrm{r}}$.

3.2 Vector equations based on Newton's second law

The momentum and angular momentum according to Newton's mechanics can be expressed as

$$m\left[\dot{\boldsymbol{v}}_1+\boldsymbol{v}_2\times\boldsymbol{v}_1+\dot{\boldsymbol{v}}_2\times\boldsymbol{R}_{\mathrm{G}}+\boldsymbol{v}_2\times\left(\boldsymbol{v}_2\times\boldsymbol{R}_G\right)\right]=\boldsymbol{f}_1, \tag{20}$$

$$\boldsymbol{J}_0\dot{\boldsymbol{v}}_2+\boldsymbol{v}_2\times\left(\boldsymbol{J}_0\boldsymbol{v}_2\right)+m\boldsymbol{R}_{\mathrm{G}}\times\left(\dot{\boldsymbol{v}}_1+\boldsymbol{v}_2\times\boldsymbol{v}_1\right)=\boldsymbol{f}_2, \tag{21}$$

where m is the quality of the vectored thruster AUV, $\boldsymbol{J}_0$ is the inertia tensor of the vectored thruster AUV in body-fixed coordinate system.

Therefore, we can represent the dynamic equations in vectorial form as

$$\boldsymbol{M}_{\mathrm{R}}\dot{\boldsymbol{v}}+\boldsymbol{C}_{\mathrm{R}}\left(\boldsymbol{v}\right)\boldsymbol{v}=\boldsymbol{f}_{\mathrm{R}}, \tag{22}$$

$$\boldsymbol{f}_{\mathrm{R}}=\boldsymbol{f}_{\mathrm{H}}+\boldsymbol{f}_{\mathrm{T}}+\boldsymbol{f}_{\mathrm{C}}+\boldsymbol{f}_{\mathrm{W}}, \tag{23}$$

where $\boldsymbol{M}_{\mathrm{R}}$ is the rigid-body inertia matrix, $\boldsymbol{C}_{\mathrm{R}}(\boldsymbol{v})$ is the rigid-body Coriolis and centripetal matrix, $\boldsymbol{f}_{\mathrm{R}}$ is the total forces and moments, $\boldsymbol{f}_{\mathrm{H}}$ is the hydrodynamic forces and moments, $\boldsymbol{f}_{\mathrm{T}}$ is the control forces and moments, $\boldsymbol{f}_{\mathrm{T}}=\boldsymbol{f}_{\mathrm{p}}+\boldsymbol{f}_{\mathrm{r}}$, $\boldsymbol{f}_{\mathrm{C}}$ is the ocean currents forces and moments, $\boldsymbol{f}_{\mathrm{W}}$ is the waves forces and moments. The disturbance caused by the waves is usually ignored when the AUVs navigate in deep water. In this paper, the complicated state of the vectored thruster AUV navigates near water surface is computed, where the waves are considered.

Moreover,

$$\boldsymbol{M}_{\mathrm{R}}\dot{\boldsymbol{v}}=\begin{pmatrix}m\dot{\boldsymbol{v}}_1+m\dot{\boldsymbol{v}}_2\times\boldsymbol{R}_{\mathrm{G}}\\ \boldsymbol{J}_0\dot{\boldsymbol{v}}_2+m\boldsymbol{R}_{\mathrm{G}}\times\dot{\boldsymbol{v}}_1\end{pmatrix}, \tag{24}$$

$$\boldsymbol{C}_{\mathrm{R}}\left(\boldsymbol{v}\right)\boldsymbol{v}=\begin{pmatrix}m\boldsymbol{v}_2\times\boldsymbol{v}_1+m\boldsymbol{v}_2\times\left(\boldsymbol{v}_2\times\boldsymbol{R}_{\mathrm{G}}\right)\\ \boldsymbol{v}_2\times\left(\boldsymbol{J}_0\boldsymbol{v}_2\right)+m\boldsymbol{R}_{\mathrm{G}}\times\left(\boldsymbol{v}_2\times\boldsymbol{v}_1\right)\end{pmatrix}. \tag{25}$$

According to that $\boldsymbol{a}\times\boldsymbol{b}=\boldsymbol{S}(\boldsymbol{a})\cdot\boldsymbol{b}$, the following expressions are obtained:

$$\boldsymbol{M}_{\mathrm{R}}=\begin{pmatrix}m\boldsymbol{I}_{3\times3} & -m\boldsymbol{S}\left(\boldsymbol{R}_{\mathrm{G}}\right)\\ m\boldsymbol{S}\left(\boldsymbol{R}_{\mathrm{G}}\right) & \boldsymbol{J}_0\end{pmatrix},$$

$$\boldsymbol{C}_{\mathrm{R}}=\begin{pmatrix}\boldsymbol{O}_{3\times3} & -m\boldsymbol{S}\left(\boldsymbol{v}_1\right)-m\boldsymbol{S}\left(\boldsymbol{v}_2\right)\boldsymbol{S}\left(\boldsymbol{R}_{\mathrm{G}}\right)\\ -m\boldsymbol{S}\left(\boldsymbol{v}_1\right)+m\boldsymbol{S}\left(\boldsymbol{R}_{\mathrm{G}}\right)\boldsymbol{S}\left(\boldsymbol{v}_2\right) & -\boldsymbol{S}\left(\boldsymbol{J}_0\boldsymbol{v}_2\right)\end{pmatrix},$$

where $\boldsymbol{S}\left(\boldsymbol{a}\right)=\begin{pmatrix}0 & -a_3 & a_2\\ a_3 & 0 & -a_1\\ -a_2 & a_1 & 0\end{pmatrix}$.

The hydrodynamic forces and moments on the vectored thruster AUV can be expressed as

$$\boldsymbol{f}_{\mathrm{H}}=-\boldsymbol{M}_{\mathrm{A}}\dot{\boldsymbol{v}}-\boldsymbol{C}_{\mathrm{A}}\left(\boldsymbol{v}\right)\boldsymbol{v}-\boldsymbol{D}\left(\boldsymbol{v}\right)\boldsymbol{v}-\boldsymbol{g}\left(\boldsymbol{\eta}\right), \tag{26}$$

where $\boldsymbol{M}_{\mathrm{A}}=\begin{pmatrix}\boldsymbol{M}_{11} & \boldsymbol{M}_{12}\\ \boldsymbol{M}_{21} & \boldsymbol{M}_{22}\end{pmatrix}=\left(\lambda_{ij}\right)$, ($i$=1…6, j=1…6) is the added mass matrix, $\boldsymbol{C}_{\mathrm{A}}\left(\boldsymbol{v}\right)$ is the hydrodynamic Coriolis and centripetal matrix, $\boldsymbol{D}\left(\boldsymbol{v}\right)$ is the hydrodynamic damping matrix.

The total hydrodynamic damping is mainly caused by radiation-induced potential damping and viscous damping. The viscous damping consists of friction damping, wave drift damping and vortex shedding damping. The total hydrodynamic damping $\boldsymbol{D}(\boldsymbol{v})\boldsymbol{v}$ is usually divided into linear part $\boldsymbol{D}_{\mathrm{L}}(\boldsymbol{v})\boldsymbol{v}$ and nonlinear part $\boldsymbol{D}_{\mathrm{NL}}(\boldsymbol{v})$, whose corresponding hydrodynamic parameters are all obtained through the experiments. The linear damping parts of the total hydrodynamic damping in the cruise mode and hover mode are the same, but the nonlinear damping parts are different. The viscous damping is the major part of the total damping when the vectored thruster AUV is in cruise mode and the linear part is larger, the non-linear part is mainly the second damping caused by friction. The two parts can be expressed as

$$\boldsymbol{D}_{\mathrm{L}}\left(\boldsymbol{v}\right)\boldsymbol{v}=-\mathrm{diag}\left(X_u,Y_v,Z_w,K_P,M_q,N_r\right)\cdot\boldsymbol{v}, \tag{27}$$

$$\boldsymbol{D}_{\mathrm{NL}}\left(\boldsymbol{v}\right)=-\mathrm{diag}\left(X_{u|u|}|u|,Y_{v|v|}|v|,Z_{w|w|}|w|,K_{p|p|}|p|,M_{q|q|}|q|,N_{r|r|}|r|\right)\cdot\boldsymbol{v}. \tag{28}$$

The vertical and horizontal motion of the vectored thruster AUV in hover mode works in the state of a large angle of attack or angle of sideslip, the nonlinear part of the fluid viscous damping plays a major role. The nonlinear damping mainly represents transverse flow resistance. The transverse flow velocity function of the any point in the body-fixed coordinate system can be defined as[13]

$$U_{\mathrm{cf}}=\sqrt{\left(v+xr\right)^{2}+\left(w-xq\right)^{2}}\ . \tag{29}$$

The corresponding damping forces can be ignored since the axial motion and rolling around the longitudinal axis of the vectored thruster AUV in hover mode is little. So the total fluid damping forces based on strip theory can be expressed as follows:

$$\begin{cases} Y_{\mathrm{h}}=-\dfrac{\rho}{2}\displaystyle\int_{x_{\mathrm{tail}}}^{x_{\mathrm{nose}}}\left[C_{\mathrm{dy}}h(x)(v+xr)^{2}+C_{\mathrm{dz}}b(x)(w-xq)^{2}\right]\cdot\frac{(v+xr)}{(U_{\mathrm{cf}}(x))}\mathrm{d}x \\ Z_{\mathrm{h}}=\dfrac{\rho}{2}\displaystyle\int_{x_{\mathrm{tail}}}^{x_{\mathrm{nose}}}\left[C_{\mathrm{dy}}h(x)(v+xr)^{2}+C_{\mathrm{dz}}b(x)(w-xq)^{2}\right]\cdot\frac{(w-xq)}{(U_{\mathrm{cf}}(x))}\mathrm{d}x \\ M_{\mathrm{h}}=-\dfrac{\rho}{2}\displaystyle\int_{x_{\mathrm{tail}}}^{x_{\mathrm{nose}}}\left[C_{\mathrm{dy}}h(x)(v+xr)^{2}+C_{\mathrm{dz}}b(x)(w-xq)^{2}\right]\cdot\frac{(w+xq)}{(U_{\mathrm{cf}}(x))}x\mathrm{d}x \\ N_{\mathrm{h}}=-\dfrac{\rho}{2}\displaystyle\int_{x_{\mathrm{tail}}}^{x_{\mathrm{nose}}}\left[C_{\mathrm{dy}}h(x)(v+xr)^{2}+C_{\mathrm{dz}}b(x)(w-xq)^{2}\right]\cdot\frac{(v+xr)}{(U_{\mathrm{cf}}(x))}x\mathrm{d}x \end{cases}, \tag{30}$$

where C_{dy} is the drag coefficient along lateral axis, C_{dz} is the drag coefficient along vertical axis.

Therefore, the nonlinear part of the total damping in hover mode can be written as

$$\boldsymbol{D}_{\mathrm{NL}}\left(\boldsymbol{v}\right)=-\left(0,Y_{\mathrm{h}},Z_{\mathrm{h}},0,M_{\mathrm{h}},N_{\mathrm{h}}\right)^{\mathrm{T}}. \tag{31}$$

The added mass can be considered as a constant which is independent of wave frequency as for the vectored thruster AUV. Therefore, the added mass matrix $\boldsymbol{M}_{\mathrm{A}}$ and the hydrodynamic Coriolis and centripetal matrix $\boldsymbol{C}_{\mathrm{A}}(\boldsymbol{v})$ can be deduced through the fluid kinetic energy. The fluid kinetic energy of the added mass is written as

$$\boldsymbol{T}_{\mathrm{A}}=\frac{1}{2}\boldsymbol{v}^{\mathrm{T}}\boldsymbol{M}_{\mathrm{A}}\boldsymbol{v}\ . \tag{32}$$

Applying the Kirchhoff's equations of fluid mechanics yields:

$$\frac{\mathrm{d}}{\mathrm{d}t}\left(\frac{\partial\boldsymbol{T}_{\mathrm{A}}}{\partial\boldsymbol{v}_{1}}\right)+\boldsymbol{v}_{2}\times\frac{\partial\boldsymbol{T}_{\mathrm{A}}}{\partial\boldsymbol{v}_{1}}=\boldsymbol{f}_{1}'\ , \tag{33}$$

$$\frac{\mathrm{d}}{\mathrm{d}t}\left(\frac{\partial\boldsymbol{T}_{\mathrm{A}}}{\partial\boldsymbol{v}_{2}}\right)+\boldsymbol{v}_{2}\times\frac{\partial\boldsymbol{T}_{\mathrm{A}}}{\partial\boldsymbol{v}_{2}}+\boldsymbol{v}_{1}\times\frac{\partial\boldsymbol{T}_{\mathrm{A}}}{\partial\boldsymbol{v}_{1}}=\boldsymbol{f}_{2}'\ , \tag{34}$$

where $\boldsymbol{f}_{1}'$ and $\boldsymbol{f}_{2}'$ are the forces and moments respectively suffered from the vectored thruster AUV.

Defining,

$$\frac{\partial\boldsymbol{T}_{\mathrm{A}}}{\partial\boldsymbol{v}_{1}}=\boldsymbol{M}_{11}\boldsymbol{v}_{1}+\boldsymbol{M}_{12}\boldsymbol{v}_{2}\quad\frac{\partial\boldsymbol{T}_{\mathrm{A}}}{\partial\boldsymbol{v}_{2}}=\boldsymbol{M}_{21}\boldsymbol{v}_{1}+\boldsymbol{M}_{22}\boldsymbol{v}_{2},$$

$$\boldsymbol{C}_{\mathrm{A}}\left(\boldsymbol{v}\right)\boldsymbol{v}=\begin{pmatrix}\boldsymbol{v}_{2}\times\dfrac{\partial\boldsymbol{T}}{\partial\boldsymbol{v}_{1}}\\ \boldsymbol{v}_{2}\times\dfrac{\partial\boldsymbol{T}}{\partial\boldsymbol{v}_{2}}+\boldsymbol{v}_{1}\times\dfrac{\partial\boldsymbol{T}}{\partial\boldsymbol{v}_{1}}\end{pmatrix}=\begin{pmatrix}\boldsymbol{0}_{3\times3} & -\boldsymbol{S}\left(\dfrac{\partial\boldsymbol{T}}{\partial\boldsymbol{v}_{1}}\right)\\ -\boldsymbol{S}\left(\dfrac{\partial\boldsymbol{T}}{\partial\boldsymbol{v}_{1}}\right) & -\boldsymbol{S}\left(\dfrac{\partial\boldsymbol{T}}{\partial\boldsymbol{v}_{2}}\right)\end{pmatrix}\begin{pmatrix}\boldsymbol{v}_{1}\\ \boldsymbol{v}_{2}\end{pmatrix},$$

which yields:

$$\boldsymbol{C}_{\mathrm{A}}\left(\boldsymbol{v}\right)=\begin{pmatrix}\boldsymbol{0}_{3\times3} & -\boldsymbol{S}\left(\boldsymbol{M}_{11}\boldsymbol{v}_{1}+\boldsymbol{M}_{12}\boldsymbol{v}_{2}\right)\\ -\boldsymbol{S}\left(\boldsymbol{M}_{11}\boldsymbol{v}_{1}+\boldsymbol{M}_{12}\boldsymbol{v}_{2}\right) & -\boldsymbol{S}\left(\boldsymbol{M}_{21}\boldsymbol{v}_{1}+\boldsymbol{M}_{22}\boldsymbol{v}_{2}\right)\end{pmatrix}. \tag{35}$$

From Eq. (22) with Eq. (23) and Eq. (26), the six-DOF dynamic equations of motion can be expressed as

$$\boldsymbol{M}\dot{\boldsymbol{v}}+\boldsymbol{C}\left(\boldsymbol{v}\right)\boldsymbol{v}+\boldsymbol{D}\left(\boldsymbol{v}\right)\boldsymbol{v}+\boldsymbol{g}\left(\boldsymbol{\eta}\right)=\boldsymbol{f}_{\mathrm{T}}+\boldsymbol{f}_{\mathrm{C}}+\boldsymbol{f}_{\mathrm{W}}\ , \tag{36}$$

where $\boldsymbol{M}=\boldsymbol{M}_{\mathrm{R}}+\boldsymbol{M}_{\mathrm{A}}$, $\boldsymbol{C}\left(\boldsymbol{v}\right)=\boldsymbol{C}_{\mathrm{R}}\left(\boldsymbol{v}\right)+\boldsymbol{C}_{\mathrm{A}}\left(\boldsymbol{v}\right)$.

The derivative of the kinematic Eq. (6) can be written as

$$\ddot{\boldsymbol{\eta}}=\boldsymbol{J}\left(\boldsymbol{\eta}\right)\dot{\boldsymbol{v}}+\dot{\boldsymbol{J}}\left(\boldsymbol{\eta}\right)\boldsymbol{v}\ . \tag{37}$$

Hence,

$$\boldsymbol{v}=\boldsymbol{J}^{-1}\left(\boldsymbol{\eta}\right)\dot{\boldsymbol{\eta}}\ , \tag{38}$$

$$\dot{\boldsymbol{v}}=\boldsymbol{J}^{-1}\left(\boldsymbol{\eta}\right)\left[\ddot{\boldsymbol{\eta}}-\dot{\boldsymbol{J}}\left(\boldsymbol{\eta}\right)\boldsymbol{J}^{-1}\left(\boldsymbol{\eta}\right)\dot{\boldsymbol{\eta}}\right]. \tag{39}$$

From Eq. (33) and Eq. (34) together with Eq. (38) and Eq. (39), the six-DOF dynamic equations of motion in the inertial coordinate system can be expressed as

$$\boldsymbol{M}_{\eta}\left(\boldsymbol{\eta}\right)\ddot{\boldsymbol{\eta}}+\boldsymbol{C}_{\eta}\left(\boldsymbol{v},\boldsymbol{\eta}\right)\dot{\boldsymbol{\eta}}+\boldsymbol{D}_{\eta}\left(\boldsymbol{v},\boldsymbol{\eta}\right)\dot{\boldsymbol{\eta}}+\boldsymbol{g}_{\eta}\left(\boldsymbol{\eta}\right)=\boldsymbol{f}_{\mathrm{T}\eta}+\boldsymbol{f}_{\mathrm{C}\eta}+\boldsymbol{f}_{\mathrm{W}\eta}. \tag{40}$$

where $\boldsymbol{C}_{\eta}\left(\boldsymbol{v},\boldsymbol{\eta}\right)=\boldsymbol{J}^{-\mathrm{T}}\left(\boldsymbol{\eta}\right)\left[\boldsymbol{C}\left(\boldsymbol{v}\right)-\boldsymbol{M}\boldsymbol{J}^{-1}\left(\boldsymbol{\eta}\right)\dot{\boldsymbol{J}}\left(\boldsymbol{\eta}\right)\right]\boldsymbol{J}^{-1}\left(\boldsymbol{\eta}\right)$,
$\boldsymbol{M}_{\eta}\left(\boldsymbol{\eta}\right)=\boldsymbol{J}^{-\mathrm{T}}\left(\boldsymbol{\eta}\right)\boldsymbol{M}\boldsymbol{J}^{-1}\left(\boldsymbol{\eta}\right)$, $\boldsymbol{D}_{\eta}\left(\boldsymbol{v},\boldsymbol{\eta}\right)=\boldsymbol{J}^{-\mathrm{T}}\left(\boldsymbol{\eta}\right)\boldsymbol{D}\left(\boldsymbol{v}\right)\boldsymbol{J}^{-1}\left(\boldsymbol{\eta}\right)$,
$\boldsymbol{g}_{\eta}\left(\boldsymbol{\eta}\right)=\boldsymbol{J}^{-\mathrm{T}}\left(\boldsymbol{\eta}\right)\boldsymbol{g}\left(\boldsymbol{\eta}\right)$, $\boldsymbol{f}_{\mathrm{T}\eta}\left(\boldsymbol{\eta}\right)=\boldsymbol{J}^{-\mathrm{T}}\left(\boldsymbol{\eta}\right)\boldsymbol{f}_{\mathrm{T}}$,
$\boldsymbol{f}_{\mathrm{C}\eta}\left(\boldsymbol{\eta}\right)=\boldsymbol{J}^{-\mathrm{T}}\left(\boldsymbol{\eta}\right)\boldsymbol{f}_{\mathrm{C}}$, $\boldsymbol{f}_{\mathrm{W}\eta}\left(\boldsymbol{\eta}\right)=\boldsymbol{J}^{-\mathrm{T}}\left(\boldsymbol{\eta}\right)\boldsymbol{f}_{\mathrm{W}}$.

3.3 Vector equations based on Lagrangian method

In order to further validate the accuracy of dynamic model, the Lagrangian method is used to deduce the six-DOF nonlinear dynamic model of the vectored thruster AUV.

Application of Lagrangian principle yields the following expression, that is

$$\frac{d}{dt}\left(\frac{\partial\boldsymbol{L}}{\partial\dot{\boldsymbol{\eta}}}\right)-\frac{\partial\boldsymbol{L}}{\partial\boldsymbol{\eta}}+\frac{\partial\boldsymbol{P}_{\mathrm{d}}}{\partial\dot{\boldsymbol{\eta}}}=\boldsymbol{f}_{\mathrm{T}\eta}+\boldsymbol{f}_{\mathrm{C}\eta}+\boldsymbol{f}_{\mathrm{W}\eta}\ , \tag{41}$$

where $\boldsymbol{P}_{\mathrm{d}}$ is the power function, the fluid dissipative force is

expressed as $\frac{\partial \boldsymbol{P}_{\mathrm{d}}}{\partial \dot{\boldsymbol{\eta}}}=\boldsymbol{D}_{\eta}(\boldsymbol{v}, \boldsymbol{\eta}) \dot{\boldsymbol{\eta}}$, the Lagrangian is written as $\boldsymbol{L}=\boldsymbol{T}_{\mathrm{R}}+\boldsymbol{T}_{\mathrm{A}}-\boldsymbol{V}$, $\boldsymbol{T}_{\mathrm{R}}$ is the vectored thruster AUV kinetic energy, $\boldsymbol{T}_{\mathrm{A}}$ is the fluid kinetic energy, $\boldsymbol{V}$ is the potential energy defined implicit by $\frac{\partial \boldsymbol{V}}{\partial \boldsymbol{\eta}}=\boldsymbol{g}_{\eta}(\boldsymbol{\eta})$.

Hence, The total kinetic energy can be expressed as

$$\boldsymbol{T}=\boldsymbol{T}_{\mathrm{R}}+\boldsymbol{T}_{\mathrm{A}}=\frac{1}{2} \dot{\boldsymbol{\eta}}^{T} \boldsymbol{M}_{\eta}(\boldsymbol{\eta}) \dot{\boldsymbol{\eta}} . \tag{42}$$

Furthermore, we can compute:

$$\frac{d}{d t}\left(\frac{\partial \boldsymbol{L}}{\partial \dot{\boldsymbol{\eta}}}\right)=\boldsymbol{M}_{\eta}(\boldsymbol{\eta}) \ddot{\boldsymbol{\eta}}+\dot{\boldsymbol{M}}_{\eta}(\boldsymbol{\eta}) \dot{\boldsymbol{\eta}}, \tag{43}$$

$$\frac{\partial \boldsymbol{L}}{\partial \boldsymbol{\eta}}=\frac{\partial \boldsymbol{T}}{\partial \boldsymbol{\eta}}-\frac{\partial \boldsymbol{V}}{\partial \boldsymbol{\eta}}=\frac{1}{2} \dot{\boldsymbol{\eta}}^{\mathrm{T}} \frac{\partial \boldsymbol{M}_{\eta}(\boldsymbol{\eta})}{\partial \boldsymbol{\eta}} \dot{\boldsymbol{\eta}}-\boldsymbol{g}_{\eta}(\boldsymbol{\eta}) . \tag{44}$$

From

$$\dot{\boldsymbol{M}}_{\eta}(\boldsymbol{\eta})=\dot{\boldsymbol{\eta}}^{\mathrm{T}} \frac{\partial \boldsymbol{M}_{\eta}(\boldsymbol{\eta})}{\partial \boldsymbol{\eta}}$$

and the Coriolis and centripetal matrix

$$\boldsymbol{C}_{\eta}(\boldsymbol{v}, \boldsymbol{\eta})=\frac{1}{2} \dot{\boldsymbol{M}}_{\eta}(\boldsymbol{\eta})$$

together with Eqs. (41), (43), (44), the six-DOF dynamic equations of motion in the inertial coordinate system can be expressed as

$$\boldsymbol{M}_{\eta}(\boldsymbol{\eta}) \ddot{\boldsymbol{\eta}}+\boldsymbol{C}_{\eta}(\boldsymbol{v}, \boldsymbol{\eta}) \dot{\boldsymbol{\eta}}+\boldsymbol{D}_{\eta}(\boldsymbol{v}, \boldsymbol{\eta}) \dot{\boldsymbol{\eta}}+\boldsymbol{g}_{\eta}(\boldsymbol{\eta})=\boldsymbol{f}_{\mathrm{T} \eta}+\boldsymbol{f}_{\mathrm{C} \eta}+\boldsymbol{f}_{\mathrm{W} \eta} . \tag{45}$$

The six-DOF nonlinear dynamic equations of the vectored thruster AUV deduced based on the Newton second law and Lagrangian approach are completely same, which shows that the dynamic model of the vectored thruster AUV is accurate and it can be used to study the motion and control system of the vectored thruster AUV.

3.4 Mathematical model of low-frequency motion

The low-frequency motion of the vectored thruster AUV is mainly caused by ocean current, second-order wave force and propulsion. The ocean current can be regarded as the circulation system in the horizontal and vertical direction which caused by gravity, wind friction and changes in water density. It is a low-frequency slow process of change. The speed of ocean current is usually defined in the n-coordinate system and described by flow axis, so the ocean current vector can be written as $(V_{\mathrm{c}}, 0, 0)^{\mathrm{T}}$. The three-dimensional ocean current speed in inertia coordinate system can be determined through two times rotations, that is

$$\begin{pmatrix} u_{\mathrm{c}}^{\mathrm{e}} \\ v_{\mathrm{c}}^{\mathrm{e}} \\ w_{\mathrm{c}}^{\mathrm{e}} \end{pmatrix}=\begin{pmatrix} \cos \alpha_{\mathrm{c}} & 0 & -\sin \alpha_{\mathrm{c}} \\ 0 & 1 & 0 \\ \sin \alpha_{\mathrm{c}} & 0 & \cos \alpha_{\mathrm{c}} \end{pmatrix}\begin{pmatrix} \cos \beta_{\mathrm{c}} & -\sin \beta_{\mathrm{c}} & 0 \\ \sin \beta_{\mathrm{c}} & \cos \beta_{\mathrm{c}} & 0 \\ 0 & 0 & 1 \end{pmatrix}\begin{pmatrix} V_{\mathrm{c}} \\ 0 \\ 0 \end{pmatrix}, \tag{46}$$

where α_{c} is the flow axis's angle of attack, β_{c} is the flow axis's angle of sideslip.

The flow velocity $\boldsymbol{v}_{\mathrm{c}}^{\mathrm{e}}$ in the inertial coordinate system is transformed into the flow velocity $\boldsymbol{v}_{\mathrm{c}}^{\mathrm{b}}$ in the body-fixed coordinate system using the Euler angles transformation matrix:

$$\boldsymbol{v}_{\mathrm{c}}^{\mathrm{b}}=\begin{pmatrix} u_{\mathrm{c}}^{\mathrm{b}} \\ v_{\mathrm{c}}^{\mathrm{b}} \\ w_{\mathrm{c}}^{\mathrm{b}} \end{pmatrix}=\boldsymbol{J}_{1}\left(\boldsymbol{\eta}_{2}\right)^{\mathrm{T}}\begin{pmatrix} u_{\mathrm{c}}^{\mathrm{e}} \\ v_{\mathrm{c}}^{\mathrm{e}} \\ w_{\mathrm{c}}^{\mathrm{e}} \end{pmatrix} . \tag{47}$$

The velocity components V_{c} of ocean current can be represented by a Gauss - Markov random process[14]:

$$\dot{V}_{\mathrm{c}}(t)+\mu_{0} V_{\mathrm{c}}(t)=w(t), \tag{48}$$

where μ_0 is a constant, define $\mu_0 = 0$ to simulate the random process of the ocean current velocity in most cases, $w(t)$ is a zero mean Gaussian white noise process.

The current-induced forces and moments can be included in the dynamic equations of motion based on the principle of relative motion and the assumption that the fluid is irrotational. The definition of relative velocity can be written as

$$\boldsymbol{v}_{\mathrm{r}}=\left(u-u_{\mathrm{c}}^{\mathrm{b}}, v-v_{\mathrm{c}}^{\mathrm{b}}, w-w_{\mathrm{c}}^{\mathrm{b}}, p, q, r\right)^{\mathrm{T}} . \tag{49}$$

Hence, the hydrodynamic forces and moments $\boldsymbol{f}_{\mathrm{H}}$ can be expressed as

$$\boldsymbol{f}_{\mathrm{H}}=-\boldsymbol{M}_{\mathrm{A}} \dot{\boldsymbol{v}}_{\mathrm{r}}-\boldsymbol{C}_{\mathrm{A}}\left(\boldsymbol{v}_{\mathrm{r}}\right) \boldsymbol{v}_{\mathrm{r}}-\boldsymbol{D}\left(\boldsymbol{v}_{\mathrm{r}}\right) \boldsymbol{v}_{\mathrm{r}}-\boldsymbol{g}(\boldsymbol{\eta}) . \tag{50}$$

where the body-fixed current velocity is usually assumed to be slowly varying such that it yields $\dot{\boldsymbol{v}}_{\mathrm{c}} \approx 0$.

The second-order wave drift force in the x, y and z directions can be modeled by three slowly-varying parameters:

$$\boldsymbol{d}=\left(d_{1}, d_{2}, d_{3}, 0, 0, 0\right)^{\mathrm{T}} . \tag{51}$$

Hence,

$$\dot{d}_{i}=w_{\mathrm{d}}, \quad (i=1,2,3) \tag{52}$$

where w_d is a zero mean Gaussian white noise process.

Finally, the mathematical model of low-frequency motion can be expressed as

$$\boldsymbol{M}\dot{\boldsymbol{v}}+\boldsymbol{C}_{\mathrm{R}}(\boldsymbol{v})\boldsymbol{v}+\boldsymbol{C}_{\mathrm{A}}(\boldsymbol{v}_{\mathrm{r}})\boldsymbol{v}_{\mathrm{r}}+\boldsymbol{D}(\boldsymbol{v}_{\mathrm{r}})\boldsymbol{v}_{\mathrm{r}}+\boldsymbol{g}(\boldsymbol{\eta})=\boldsymbol{f}_{\mathrm{T}}+\boldsymbol{d}\ . \quad (53)$$

3.5 Mathematical model of high-frequency motion

The high-frequency motion of the vectored thruster AUV is mainly caused by the first-order wave force. The six-DOF high-frequency motion (surge, sway, heave, roll, pitch and yaw) caused by the first-order wave forces can be seen as the harmonic oscillators that adding different damping respectively. The second-order random wave transfer function is used to estimate the wave spectrum-PM spectrum[15], which is expressed as

$$h_i(s)=\frac{K_{wi}s}{s^2+2\zeta_i w_e s+w_e^2}, \quad (54)$$

where $K_{wi}=2\zeta_i w_e\sigma_w$, σ_w is the wave intensity, ζ_i is the relative damping coefficient, w_e is the encounter frequency, $w_e=w_0-\frac{w_0^2}{g}U\cos\chi$, χ is the encounter angle, w_0 is the peak frequency of PM spectrum, which is related with the significant wave height H_s: $w_0=0.40\sqrt{g/H_s}$. The high-frequency motion caused by the first-order wave forces can be expressed as

$$y_{\mathrm{H}i}(s)=h_i(s)w(s), \quad (55)$$

where $w(s)$ is a zero mean Gaussian white noise process.

Finally, the standard linear state-space model of the high-frequency motion can be expressed as

$$\dot{\boldsymbol{x}}_{\mathrm{H}}=\boldsymbol{A}_{\mathrm{H}}\boldsymbol{x}_{\mathrm{H}}+\boldsymbol{E}_{\mathrm{H}}\boldsymbol{w}_{\mathrm{H}}, \quad (56)$$

$$\boldsymbol{y}_{\mathrm{H}}=\boldsymbol{C}_{\mathrm{H}}\boldsymbol{x}_{\mathrm{H}}, \quad (57)$$

where $\boldsymbol{A}_{\mathrm{H}}=\begin{pmatrix}\boldsymbol{0}_{6\times6} & \boldsymbol{I}_{6\times6}\\ -\boldsymbol{\Omega} & -2\boldsymbol{\Lambda}\boldsymbol{\Omega}\end{pmatrix}$, $\boldsymbol{E}_{\mathrm{H}}=\begin{pmatrix}\boldsymbol{0}_{6\times6}\\ \boldsymbol{K}_w\end{pmatrix}$,

$\boldsymbol{C}_{\mathrm{H}}=(\boldsymbol{0}_{6\times6}\quad\boldsymbol{I}_{6\times6})$, $\boldsymbol{\Lambda}=\mathrm{diag}(\zeta_1,\cdots,\zeta_6)_{6\times6}$,

$\boldsymbol{\Omega}=\mathrm{diag}(w_e^2,\cdots,w_e^2)_{6\times6}$, $\boldsymbol{K}_w=\mathrm{diag}(K_{w1},\cdots,K_{w6})_{6\times6}$,

$\boldsymbol{x}_{\mathrm{H}}=(\boldsymbol{x}_{\mathrm{h}1}^{\mathrm{T}},\boldsymbol{x}_{\mathrm{h}2}^{\mathrm{T}})^{\mathrm{T}}$, $\boldsymbol{x}_{h1}=(x_{\mathrm{h}x},x_{\mathrm{h}y},x_{\mathrm{h}z},x_{\mathrm{h}\phi},x_{\mathrm{h}\theta},x_{\mathrm{h}\psi})^{\mathrm{T}}$,

$\boldsymbol{x}_{\mathrm{h}2}=\boldsymbol{y}_{\mathrm{H}}=(\xi_{\mathrm{H}},\eta_{\mathrm{H}},\zeta_{\mathrm{H}},\phi_{\mathrm{H}},\theta_{\mathrm{H}},\psi_{\mathrm{H}})^{\mathrm{T}}$, $\boldsymbol{w}_{\mathrm{H}}$ is a vector of zero mean Gaussian white noise processes.

4 Calculation and Analysis of the Position and Attitude in Complex Sea Conditions

4.1 Performance analysis of the spatial motion in interference-free environment

The dynamic model in interference-free environment is established through ignoring the ocean currents and waves disturbance based on the kinematic and dynamic equations in complex sea conditions. Then the Runge-Kutta arithmetic algorithm is used to solve the dynamic model. The inputs are the propeller speed, the space angles of vector propellers and rudder angles. The outputs is the six-DOF motion parameters such as *u*, *v*, *w*, *p*, *q* and *r*, at the same time the position and attitude parameters are obtained.

Fig. 5 shows the changes of the vectored thruster AUV's speeds at different propeller speeds. It can be seen that the vectored thruster AUV's speeds reach a steady value quickly at different propeller speeds and keep the steady increase with the increase of propeller speeds.

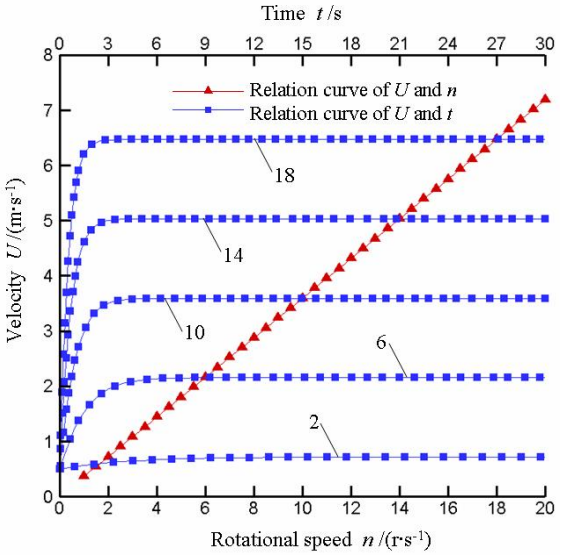

Fig. 5. Navigation speeds at different propeller speeds

The rudders are hard to achieve the course control when the vectored thruster AUV sails at low speed, while the vectored thrusters can achieve the target quickly through adjusting its space angles. Fig. 6 shows the ascending and descending trajectories of the vectored thruster AUV when the propeller speed is 5 r/s and the space angle δ_d of the vector propeller is ±90°. Since the nose of the vectored thruster AUV is streamline, so there is a positive x-axis propulsion making the vectored thruster AUV forward when it ascends and descends. When the vectored thruster AUV turns at low speed, the two bowed vector thrusters are used to offer the required propulsion through adjusting its space angle, while the two sternward vector thrusters are not used in order to avoid the phenomenon of torque offset, which reduces the steering efficiency. The right bowed vector thruster's space angle is defined as δ_r=10° and the

remaining three vector thrusters have on propeller speeds, the turning trajectory of the vectored thruster AUV is shown in Fig. 7. There is a slight dive in the turning process because of the single propeller thrust together with the fluid disturbance, which is consist with the phenomenon of Refs. [1].

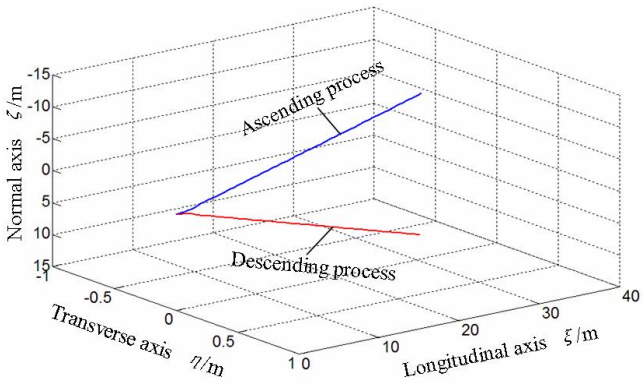

Fig. 6. Trajectories of the ascending and descending processes

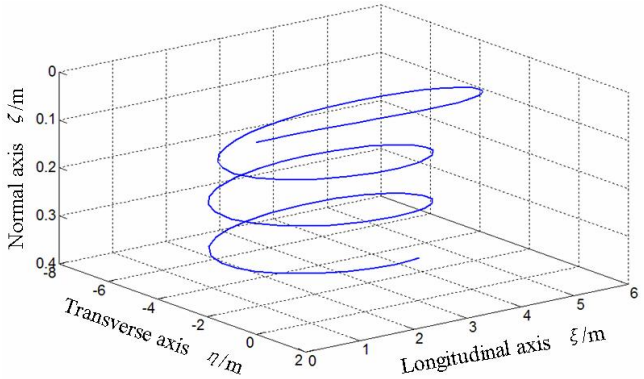

Fig. 7. Motion trajectory of the turning process

The rudders have higher efficiency to achieve the course control when the vectored thruster AUV sails at high speed according to the hydrodynamic theory. Fig. 8 shows the spiral ascending process of the vectored thruster AUV when the propeller speed n = 20 r/s, rudder angle δ_r=10° and plane angle δ_p=45°. The trajectory computed accords with the corresponding result of the input, which indicates that the dynamic model and kinematic model based on the Euler angles method are correct.

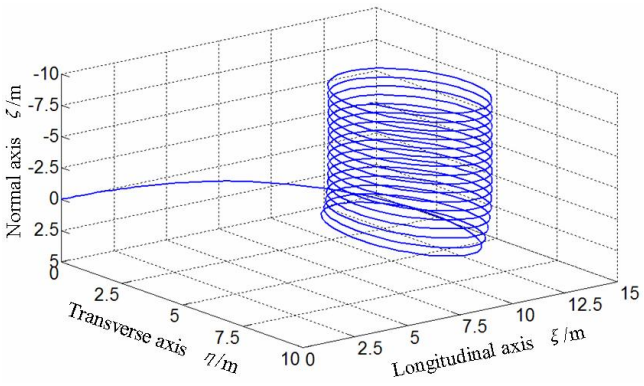

Fig. 8. Motion trajectory of the spiral ascending process

In order to verify the applicability of the quaternion method at different pitch angles, we set the initial attitude angle $(\phi,\theta,\psi)^{\mathrm{T}}=(0^{\circ},0^{\circ},0^{\circ})^{\mathrm{T}}$, which accords with the initial attitude of most AUVs. Give a constant drive orders, but not rudders control orders, until the vectored thruster AUV achieves to be in steady cruise state and then give the planes a pulse command to keep it deflects until the 60 s. The navigational trajectory of the vectored thruster AUV is computed when the three pulse amplitudes of the plane angles are 10°, 20° and 30° respectively. The input functions are shown in Fig. 9. Fig. 10 shows the trajectories for the three cases of the vectored thruster AUV when the propeller speed is 10 r/s, we can see its motion is consistent with the actual situation.

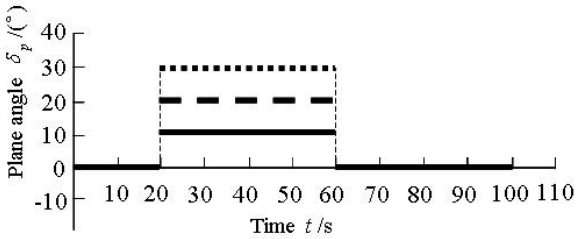

Fig. 9. Input functions of the plane angles

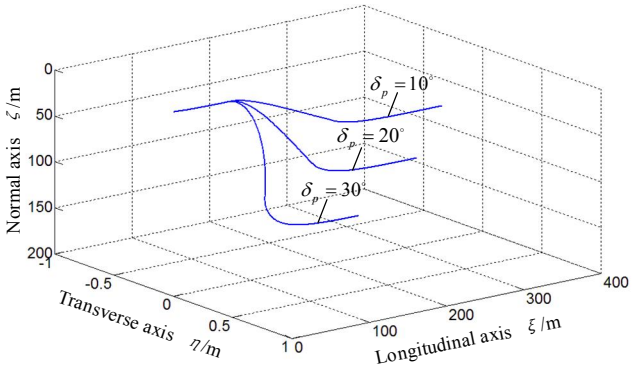

Fig. 10. Motion trajectories of the different plane angles

The navigational trajectory of the vectored thruster AUV when the pulse amplitude of the plane angle is 30° shows the superiority of the quaternion method, shown in Fig. 11. The curves of the axial velocity u and vertical velocity w tend to be stable at the 20 s. Then a plane order is given, the axial velocity u and vertical velocity w decline due to the resistance change until canceling the order at the 60 s. Finally, the axial velocity u gradually gets to be 3.59 m/s, while the vertical velocity w gets to be 0 m/s. Fig. 12 shows the curves of the pitch angle θ and pitch angle velocity q. The roll angle and the yaw angle are zero because the rudder angle is zero. The pitch angle decreases continuously from zero until passing through the point $\theta=-90^{\circ}$ under the effect of the plane. The simulation system runs accurately and the curve of the pitch angle is smooth without singular point, which proves well the feasibility of the quaternion method to solve the problem

that the simulation based on the Euler angles method can not proceed at the points $\theta = \pm 90^{\circ}$. The curves of the quaternion are shown in Fig. 13. The roll angle ϕ and yaw angle ψ are zero because ε_1 and ε_3 are zero, while ε_2 and ε_4 have a corresponding change with the pitch angle θ.

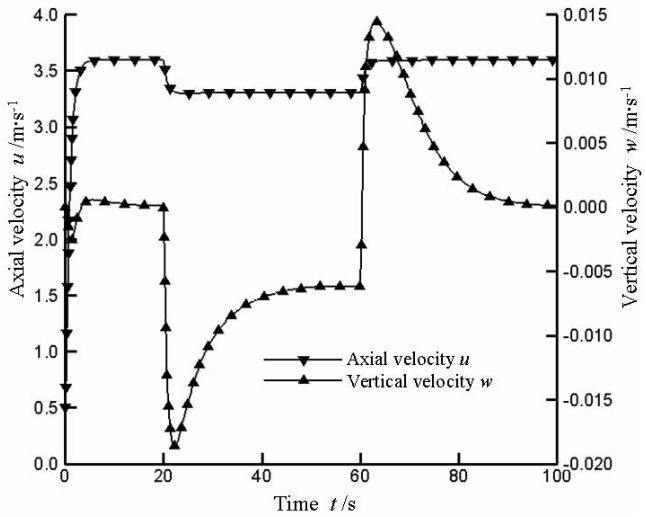

Fig. 11. Curves of the axial velocity u and vertical velocity w

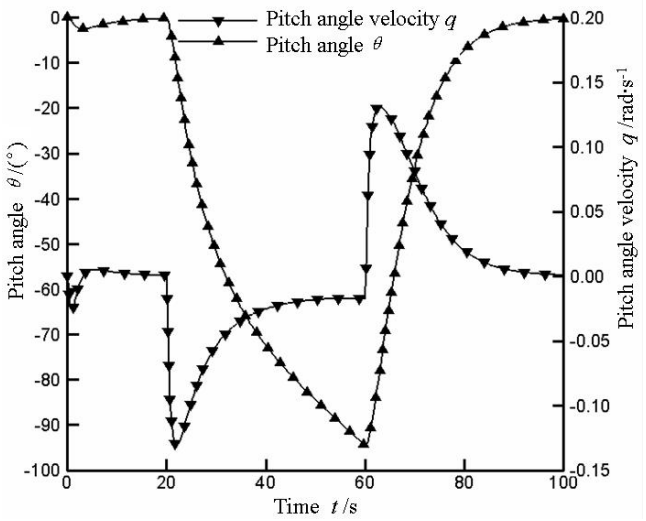

Fig. 12. Curves of the pitch angle θ and pitch angle velocity q

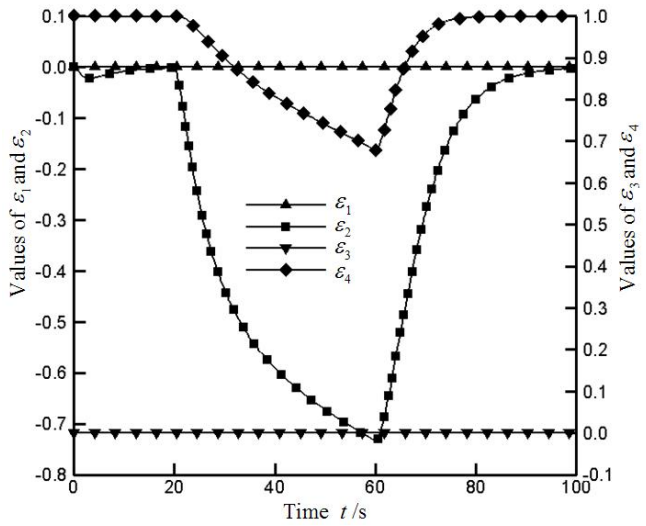

Fig. 13. Curves of the quaternion

4.2 Performance analysis of the spatial motion near water surface in environmental disturbance

The low-frequency motion model and high-frequency motion model of the vectored thruster AUV near water surface are established based on the random wave theory, which can simulate a variety of motions in the ocean current and wave disturbance together with its kinematic model. In order to design the control system of the vectored thruster AUV in environmental disturbance, the analysis of its kinetic characteristics is necessary.

The cruise state of the vectored thruster AUV in environmental disturbance is simulated through solving the kinetic and dynamic equations based on the nonlinear model proposed in this paper. Define the parameters include the propeller speed n=8 r/s, ocean wave grade S = 4, significant wave height H_s = 1.8m, flow axis's angle of attack α_c=15° and flow axis's angle of sideslip β_c=25°. The low-frequency motion signal, high-frequency motion signal and measured motion signal of the vectored thruster AUV cruising near water surface are shown in Fig. 14. The integrated motion signal is comprised of the low-frequency motion signal and high-frequency motion signal, while the measured motion signal includes the integrated motion signal and measured noise. It shows that the control of low-frequency motion signal can achieve to avoid energy wasting and propellers wearing down, so it is necessary to filter high-frequency motion signal and measured noise during the control system design. Moreover, the ruleless spiral motion appears after several seconds in complex sea conditions because the motions are not controlled, which is different with the phenomenon in interference-free environment. Therefore, in order to keep the high mobility and maneuverability of the vectored thruster AUV in complex sea conditions, an advanced autopilot should be designed.

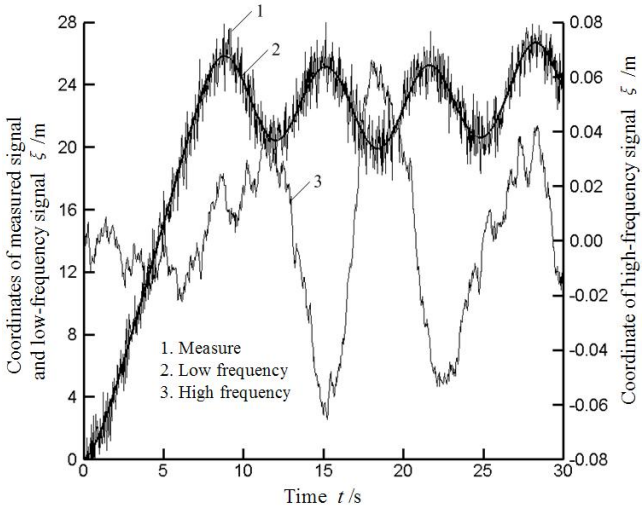

(a) Curves of the longitudinal-axis coordinate ξ

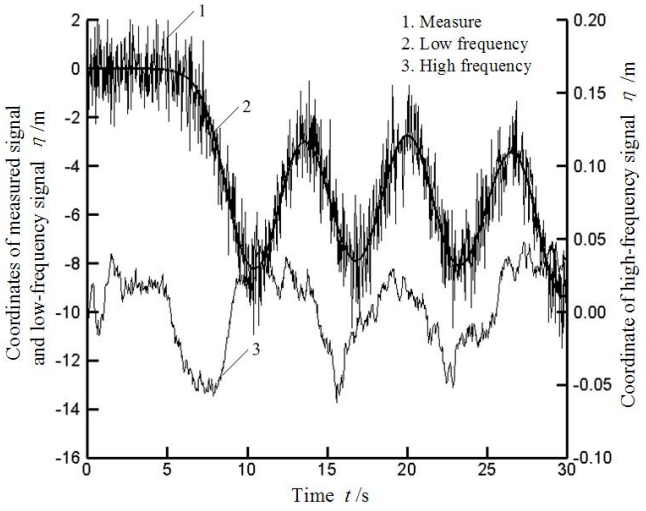

(b) Curves of the transverse-axis coordinate η

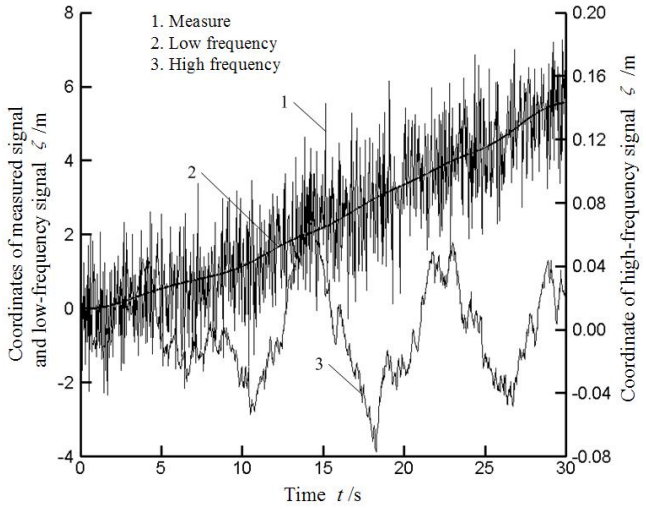

(c) Curves of the normal-axis coordinate ζ

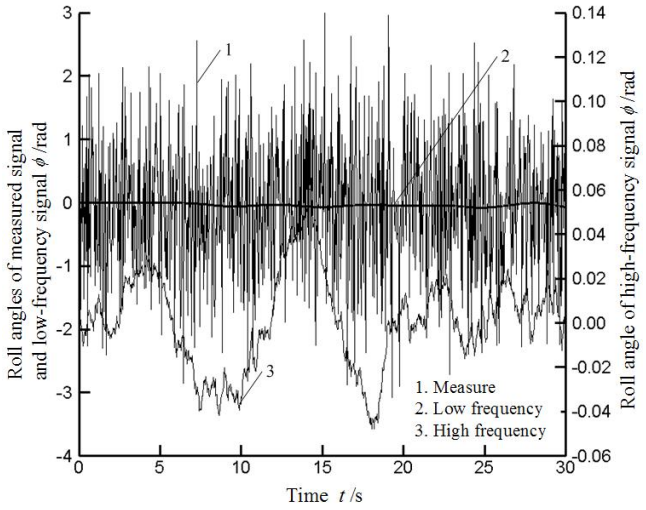

(d) Curves of the roll angle ϕ

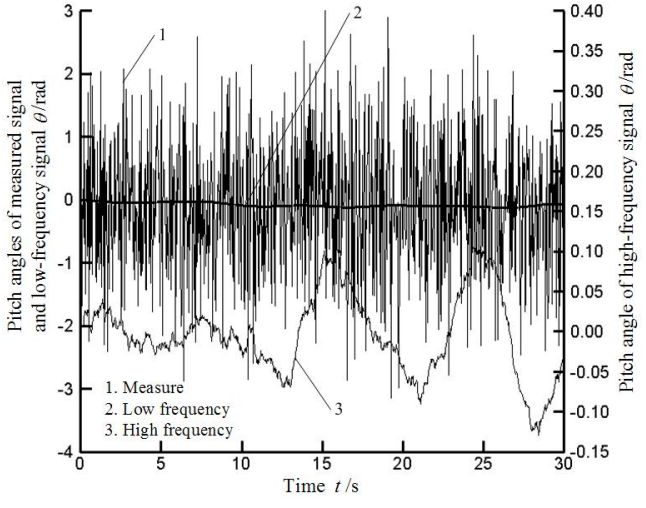

(e) Curves of the pitch angle θ

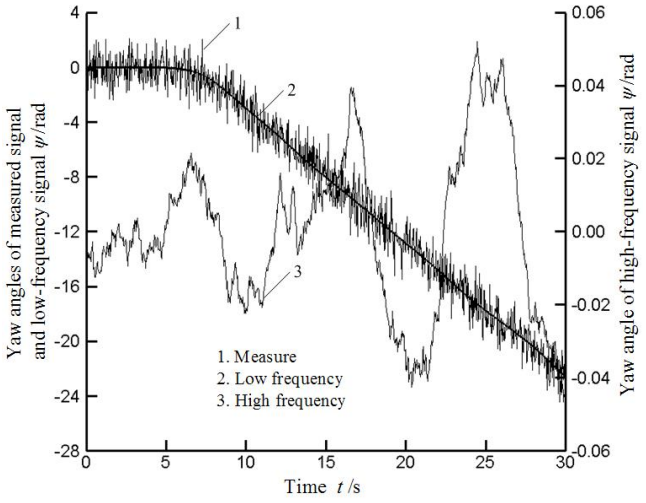

(f) Curves of the yaw angle ψ

Fig. 14. Curves of the position and attitude signals

5 Conclusions

(1) Euler angles representation is applied to establish six-DOF kinematic model according to the structural and kinetic characteristics of the vectored thruster AUV. In order to avoid especial singularities and achieve the satisfactory performance with arbitrary angles, the quaternion method is used to solve the problem that Euler angles representation is meaningless when the pitch angles are $\pm 90^{\circ}$.

(2) The Newton second law and Lagrangian approach are used to deduce the vectored thruster AUV's nonlinear dynamic equations with six degrees of freedom in complex sea conditions respectively, the dynamic models of the two methods are same, which explains that the dynamic model of the vectored thruster AUV is accurate.

(3) The Runge-Kutta arithmetic is used to solve the dynamic equations of the vectored thruster AUV in interference-free environment. The kinematic model and dynamic model are proved to be valid through the computation and analysis of its spatial motion's

performance in interference-free environment, which clears up the difficulties of computation and display of the coupled nonlinear motion equations in complex sea conditions. Moreover, it shows that the maneuverability of the vectored thruster AUV equipped with rudders and vectored thrusters is enhanced.

(4) The low-frequency motion model and high-frequency motion model of the vectored thruster AUV near water surface are established based on the random wave theory, which can simulate a variety of motions in the ocean current and wave disturbance together with its kinematic model. Then the position and attitude signals of the vectored thruster AUV in environmental disturbance are analyzed, which lays a foundation for the control system design in complex sea conditions.

References

[1] HOU W. *System control and experiments on autonomous underwater vehicle with capabilities of landing and sitting-bottom*[D]. Tianjin: Tianjin University, 2006.

[2] PAN C Y, WEN X S. Research on transmission principle and kinematic analysis for involute spherical gear [J]. *Chinese Journal of Mechanical Engineering*, 2005, 41(5): 1−9.

[3] GAO F D, PAN C Y, XU H J, et al. Design and mechanical performance analysis of a new wheel propeller [J]. *Chinese Journal of Mechanical Engineering*, 2011, 24(3): 53−60.

[4] YUH J. Design and control of autonomous underwater robots: A survey [J]. *Autonomous Robots*, 2000, 8(1): 7−24.

[5] HOU W, WANG S X, ZHANG H G. Dynamic modeling and control for miniature autonomous underwater vehicle [J]. J*ournal of Tianjin University*, 2004, 37(9): 769−773.

[6] CAO Y H, SHI X H. Trajectory tracking control and simulation of AUV [J]. *Computer Simulation*, 2006, 23(7): 19−21.

[7] YAN W S, XU D M, LI J, et al. A new method for modeling long distance autonomous underwater vehicle [J]. *Journal of Northwestern Polytechnical University*, 2004, 22(8): 500−504.

[8] CHEN H H. LI Y P. Simulation of AUV in six degrees of freedom [J]. *Control Engineering of China*, 2002, 9(6): 72−74.

[9] FOSSEN T I. *Guidance and control of ocean vehicles* [M]. New York: John Wiley and Sons Ltd, 1994.

[10] SHEPPARD S W. Quaternion from rotation matrix [J]. *Journal of Guidance and Control*, 1978, 1(3): 223−224.

[11] DONALD P B. *A virtual world for an autonomous underwater vehicle* [D]. Washington: Naval Postgraduate School, 1992.

[12] GAO F D, PAN C Y, YANG Z, et al. Numerical analysis and validation of propeller open-water performance based on CFD [J]. *Chinese Journal of Mechanical Engineering*, 2010, 46(8): 133−139.

[13] HEALEY A J, LIENARD D. Multivariable sliding mode control for autonomous diving and steering of unmanned underwater vehicle [J]. *Journal of Oceanic Engineering*, 1993, 18(3): 327−339.

[14] FOSSEN T I. *Marine control systems: guidance, navigation and control of ships, rigs and underwater vehicle* [M]. Trondheim: Marine Cybernetics AS, 2002.

[15] PIEROSN W J, MOSCOWITZ L. A proposed spectral from for fully developed wind seas based on the similarity theory of S. A. Kitaigorodskii. [J]. *Geophys. Res.*, 1964, 69(24): 5 181−5 190.

Biographical notes

GAO Fudong, born in 1982, is currently a PhD candidate at *College of Mechatronic Engineering and Automation*, *National University of Defense Technology*, *China*. He received his bachelor degree and master degree in 2005 and 2007, respectively from *National University of Defense Technology, China*. His research interests include computational fluid dynamics, design and performance prediction of submerged weapons.
Tel: +86-731-84574932; E-mail: gaofudong2005@163.com

PAN Cunyun, born in 1955, is currently a professor at *National University of Defense Technology*, *China*. His research interests include mechachonics engineering, ocean engineering and mechanical design theory.
Tel: +86-731-84576481; E-mail: pancunyun@sina.com

XU Xiaojun, born in 1972, is currently an associate professor at *National University of Defense Technology*, *China*. His research interests include mechachonics engineering, ocean engineering and robotics.
Tel: +86-731-84574932; E-mail: xuxiaojunmail@sina.com

ZHANG Xiang, born in 1973, is currently an associate professor at *National University of Defense Technology*, *China*. Her research interests include mechachonics engineering, ocean engineering and robotics.
Tel: +86-731-84574932; E-mail: zxjimmywyh@163.com